Polymer 50 (2009) 2643–2654

Contents lists available at ScienceDirect

Polymer

journal homepage: www.elsevier.com/locate/polymer

Synthesis and thermal oxidative degradation of a novel amorphous polyamide/nanoclay nanocomposite

Xingui Zhang, Leslie S. Loo*

School of Chemical and Biomedical Engineering, Nanyang Technological University, N1.2 B1-12, 62 Nanyang Drive, Singapore 637459, Singapore

ARTICLE INFO

Article history:
Received 23 December 2008
Received in revised form
16 March 2009
Accepted 4 April 2009
Available online 16 April 2009

Keywords:
Amorphous polyamide nanocomposites
Thermal oxidative degradation
Fourier transform infrared spectroscopy

ABSTRACT

A novel amorphous polyamide/montmorillonite nanocomposite based on poly(hexamethylene isophthalamide) was successfully prepared by melt intercalation. Wide angle X-ray diffraction and transmission electron microscopy showed that organoclay containing quaternary amine surfactant with phenyl groups was delaminated in the polymer matrix, resulting in well-dispersed morphologies even at high montmorillonite content. Thermal oxidation behavior of the polymer nanocomposites was studied by thermogravimetric analysis (TGA), and the chemical evolution in the solid residue was monitored by elemental analysis and Fourier transform infrared spectroscopy (FTIR). TGA results showed that the addition of well-dispersed organoclay resulted in a substantial increase (30 °C) in the onset degradation temperature of the nanocomposites as compared to the homopolymer. Elemental analysis on the solid residue indicated that the presence of nanoclay resulted in char formation with greater thermal stability. FTIR spectra showed that thermal degradation in air occurred via both oxidative and non-oxidative mechanisms simultaneously. In the homopolymer, the oxidative mechanism was more dominant. However, with the addition of well-dispersed organoclay, the non-oxidative pathway became more significant. Hence the presence of delaminated nanoclay layers could effectively retard thermo-oxidative degradation of the amorphous polymer by constraining the polymer chains and slowing down the rate of oxygen diffusion through the nanocomposites, but it was not as effective in hindering the non-oxidative degradation reaction pathway.

1. Introduction

Polymer/nanoclay nanocomposites have been extensively studied [1–5] since the Toyota research group successfully synthesized polyamide 6 nanocomposites based on montmorillonite (MMT) in 1993 [6,7]. In many cases, the addition of a small amount (ca. 5 wt%) of nanoclay to the polymer matrix was sufficient to cause remarkable improvements in mechanical properties [8], heat distortion temperature [6], thermal stability [9,10], and flame retardance [11,12]. Blumstein first reported the improved thermal stability of a polymer/MMT nanocomposite which was based on polymethyl methacrylate (PMMA) [13].

The barrier model is a widely accepted mechanism to explain the thermal property enhancement in polymer/clay nanocomposites [4,9]. However the notion of barrier effect is not limited to a silicate-enriched char layer formed on the polymer melt surface, but rather it covers the situation that the delaminated nanoclay layers spatially constrain the molecular mobility of polymer segments and hinder the diffusion of volatile decomposition products within the nanocomposites [14,15]. More recently, Chen et al. have used the notion of "nanoconfinement", which is conceptually identical to the notion of "barrier", to study the fundamental effects of nanoclay on the enhanced thermal behavior of polymer nanocomposites [16]. Consequently, in order to enhance the barrier effect as well as the nanoconfinement effect, the clay surface was often modified with an organic surfactant to improve the interactions between the clay particles and the polymer in order to obtain a nanocomposite with well-dispersed nanofiller morphology [17–20].

Generally, it has been shown that the thermal stability of polyamide 6 or polyamide 66, as indicated by the initial temperature of decomposition in a nitrogen atmosphere, did not improve (and sometimes worsened) with the addition of nanoclay [21–25]. For example, in well-exfoliated polyamide 66 nanocomposite with 5 wt% organic MMT, Qin et al. found that the decomposition temperature of the nanocomposite was 10 °C lower than that of pure polyamide 66 (445.8 °C) in a nitrogen atmosphere, but 7 °C higher than that of the polymer matrix (440.4 °C) when the degradation took place in air [22]. They attributed this difference to

* Corresponding author. Tel.: +65 6790 6737; fax: +65 6794 7553.
E-mail address: ssloo@ntu.edu.sg (L.S. Loo).

0032-3861/$ – see front matter © 2009 Elsevier Ltd. All rights reserved.
doi:10.1016/j.polymer.2009.04.011

the barrier effect of nanoclay layers in the presence of oxygen. Similar phenomena were also observed in non-charring polyethylene (PE) or poly(ethylene-*co*-vinyl acetate) (EVA)/organic MMT systems [18,26].

Unlike thermal degradation in the absence of oxygen, where bond scission occurs randomly, oxidative degradation is characterized by random scission of the polymer backbone [27]. The key issues in the thermal oxidative degradation of polymer systems are: (a) the sites where oxidation occurs, (b) the type of structural fragments which is most vulnerable to degradation, (c) the means by which the polymer matrix should be protected against thermal degradation, and (d) the main principle behind the protection [27]. Studies in the thermal oxidation of polymer/clay nanocomoposites are important because many such materials are required in applications which involve prolonged service in air at high temperatures. Hence, knowledge of the onset degradation temperature, the resulting degradation products, and the polymer degradation mechanism in the presence of nanoclay and oxygen are critical in order to design polymer nanocomposites with superior thermal properties [23]. Currently, much of the research on the thermal or thermo-oxidative degradation of polymer/nanoclay nanocomposites have focused on analyzing the gaseous decomposition products evolved during the degradation process. Such analysis was accomplished through the use of hyphenated techniques such as TGA combined with mass spectrometry and FTIR (TGA/MS and TGA/FTIR), as well as pyrolysis-gas chromatography combined with MS (pyrolysis-GC/MS) [11,16,24,27,28]. Although these studies revealed valuable indirect information on the chemistry of the degradation process, they were not able to provide direct information on the chemical changes undergone by the solid materials upon thermal degradation [24,26,29]. In fact, drawing conclusions from such indirect evidence alone could lead to contradictory and sometimes erroneous conclusions. For instance, during thermal decomposition in nitrogen, Pramoda et al. found that the functionalities of the evolved products analyzed by TGA/FTIR were similar for both polyamide 6 and its nanoclay nanocomposites. Hence they concluded that the presence of nanoclay would not affect the degradation pathway of polyamide 6 [30]. However, in another similar study, Jang and Wilkie used GC/MS to analyze the evolved condensable products of polyamide 6 and its nanoclay nanocomposites and found some differences. Hence they conjectured that the degradation pathway of polyamide 6 had been modified in the presence of clay [24]. They then tried to confirm their hypothesis by analyzing the solid residue of pure polyamide 6 and its nanocomposites at 40 wt% mass loss using FTIR, but the infrared spectra did not present sufficient information to indicate that chemical changes had occurred in the residue during the degradation process. Jang and Wilkie, however, did not examine the residue at other mass losses. Hence, in order to fully ascertain the role of nanoclay during thermal decomposition, it is also important to study the changes in the chemical composition and structure of the solid residue formed at various temperatures [27]. Recently, Chen and Vyazovkin reported the FTIR analysis of the gas-phase and condensed-phase degradation products of polystyrene (PS) and its nanocomposites, and concluded that the PS/clay nanocomposites exhibited greater stability under thermal oxidation than PS [31]. To the author's knowledge, however, very little investigation of this nature has been carried out, particularly for polyamide systems [24,26].

In this paper, the thermo-oxidative stability of a novel melt processed nanocomposite based on an amorphous semi-aromatic polyamide, poly(hexamethylene isophthalamide), is presented. This polymer is commonly known as polyamide 6I. Very little research has been carried out on amorphous polyamide/nanoclay nanocomposites, although there exists quite a large literature for melt processed nanocomposites based on aliphatic semicrystalline polyamides, including studies on their thermal stability [24,30,32,33]. At first glance, it may seem unusual to choose this inherently complex amorphous polyamide for the study, but it must be emphasized that this was a deliberate choice. First, using a fully amorphous polyamide would remove the complications that would arise due to the presence of a crystalline phase or nanoclay-induced crystalline phase transitions (which is common in semicrystalline polyamides) [34,35]. Second, as discussed later, the FTIR spectrum of the amorphous polyamide is remarkably straightforward and easy to interpret [36]. In many applications, poly(hexamethylene isophthalamide) is advantageous over semicrystalline polyamides because of its optical transparency, good electrical insulation properties, good chemical resistance and low moisture absorption [37–39]. This high-performance material is used as transparent covers and panes in the electrical industry and as packaging materials in polymer blends [40–42]. Therefore, successful synthesis of a novel amorphous polyamide/clay nanocomposite with enhanced thermal properties could broaden the scope of applications of this polymer.

The objective of this work is to gain insight into the chemical transformations and decomposition process of this polymer nanocomposite during thermal oxidation. Thermal analysis (TGA/DTG) was used to identify the different stages of degradation. Elemental analysis (EA) and FTIR were performed on the solid residue obtained at various temperatures in order to provide direct information about the chemical changes occurring in the material. Finally, an explanation to account for the improved thermal stability in such polymer nanocomposites is proposed in light of these results.

2. Experimental

2.1. Materials

The materials used in this study are listed in Table 1. The polymer was obtained from Lanxess under the product trade name Durethan T40. Fig. 1a shows the repeat unit of the amorphous polyamide (aPA). Pristine sodium montmorillonite (MMT) nanoclay and one type of MMT-based organoclay, abbreviated as NaMMT and 10AMMT respectively, were supplied by Southern Clay Products. 10AMMT contains a surfactant with a phenyl ring. The chemical structure of this surfactant is shown in Fig. 1b, where "HT" stands for hydrogenated tallow. Prior to blending, the polymer and nanoclay were first dried in a vacuum oven at 80 °C for at least 12 h. GC grade 1,1,1,3,3,3-hexafluoro-2-propanol (HFIP, 99.8% purity) and GC grade 2,2,2-trifluorethanol (TFE, 99.9% purity) were purchased from Aldrich Chemical Company and used as-received.

2.2. Melt processing

The aPA/nanoclay nanocomposites were made via a two-step process in a nitrogen atmosphere. First, a 50 g master batch of aPA containing 12 wt% MMT (wt% excludes surfactants) was prepared by melt blending the dried polymer pellets and nanoclay in a Haake

Table 1
Materials used in this study.

Material (designation used in this paper)	Supplier designation	Specifications
aPA	Durethan T40	Poly(hexamethylene isophthalamide)
NaMMT	*Cloisite*® Na^+	92.6 CEC,[a] d_{001} spacing = 1.05 nm
10AMMT	*Cloisite*® 10A:dimethyl, benzyl, hydrogenated tallow quaternary ammonium chloride organoclay	125 CEC, organic content = 36.9 wt%, d_{001} spacing = 1.95 nm

[a] CEC: cation exchange capacity, mequiv/100 g.

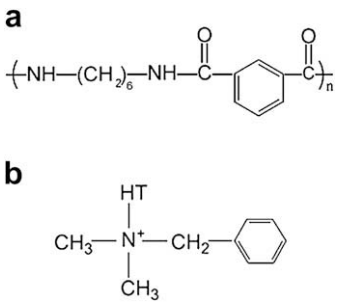

Fig. 1. Chemical structures of (a) aPA polymer, and (b) surfactant on 10AMMT.

Polydrive mixer using a mean residence time of 5 min. The mixing temperature was set at 270 °C. In the second step, appropriate amounts of dried aPA pellets were then blended with the master batch to obtain polymer nanocomposites with the requisite MMT content using the same Haake Polydrive. This was accomplished at a lower temperature of 260 °C using a mean residence time of 5 min. For aPA containing 10AMMT organoclay, polymer nanocomposites with nominal content of 1, 3, 5, 7, 10 wt% MMT (wt% excludes surfactants) were prepared. For aPA containing NaMMT, only samples containing 5 and 10 wt% MMT were made. Pure aPA samples were made by simply blending the dried polymer pellets in the first blending process at 270 °C. Finally, the pure aPA and the polymer nanocomposites were compressed into films (ca. 150 ± 5 μm) at 220 °C using a Carver Press (Model 4128). These thin films were then used for later characterizations.

The exact amount of MMT in the polymer nanocomposites was calculated by placing pre-dried materials in a furnace at 900 °C for 45 min and then weighing the remaining MMT ash. A correction for the loss of structural water was also made in the calculations [8].

2.3. Characterization

Transmission electron microscopy (TEM) was used to observe the dispersion of clay layers in the polymer matrix. Thin sections of approximately 50 nm in thickness were cut from the nanocomposites at room temperature and examined using a JEOL 3010 TEM instrument at an acceleration voltage of 200 kV.

Wide angle X-ray Diffraction (WAXD) measurements were carried out on a Siemens D5005 X-ray diffractometer using Cu Kα radiation at a scanning rate of 1°/min in the 2θ region of 2–10°.

Molecular weights of the homopolymer and nanocomposites were obtained in a Shimadzu LC20A Gel Permeation Chromatography (GPC) system using a mixed TFE/HFIP (98:2 vol%) solvent (eluent). Since GPC analysis requires that samples do not contain solid additives [43,44], the samples were first filtered though a 0.2-μm filter membrane prior to analysis [45]. A calibration curve based on polyethylene oxide standard was used [46].

TGA was carried out using a Research Instrument TGA-DTA 2950 at a heating rate of 10 °C/min from 30 °C to 800 °C under airflow. Typically, two replicates were run for each sample, and the mean was reported. The reproducibility of the measurements was ±2 °C.

Solid residue of the samples degraded to various extents was also prepared using the TGA instrument by heating the materials from 25 °C to a selected temperature in air with a heating rate of 10 °C/min, and then rapidly cooling the residue to room temperature. Residual products formed at selected temperatures of 350 °C, 400 °C, 430 °C, 450 °C, 470 °C, 480 °C, 500 °C, 550 °C and 600 °C were produced in this manner. These solid products were considered to be representative of the different decomposition stages undergone by the materials. Elemental analysis of these heat-treated samples was performed in an Elementar Vario EL III elemental analyzer for oxygen. FTIR spectra were obtained for the solid products using KBr pellets on a Nicolet Model 5700 spectrometer using a DTGS KBr detector in the range of 4000–400 cm^{-1}. Each spectrum was obtained by signal averaging a minimum of 64 scans at a resolution of 2 cm^{-1}. Baseline correction was applied to all spectra. For the nanocomposites, the Si–O stretching peak was used as internal standard to normalize all the spectra.

3. Results and discussion

3.1. Characterization of nanocomposites

X-ray diffraction (XRD) and TEM are complementary techniques which can be used to elucidate the structure and morphology of polymer nanocomposites [47]. XRD gives information about the *d*-spacing of the clay platelets while TEM shows the actual dispersion of fillers in the polymer matrix [10].

Fig. 2 shows the XRD scans for all the nanocomposites. Fig. 2a presents the X-ray results at low 2θ of the aPA nanocomposites based on 10AMMT. Pure 10AMMT powder has a prominent basal reflection at 2θ = 4.53°, corresponding to a *d*-spacing of 1.95 nm. For aPA/10AMMT nanocomposites at low filler contents

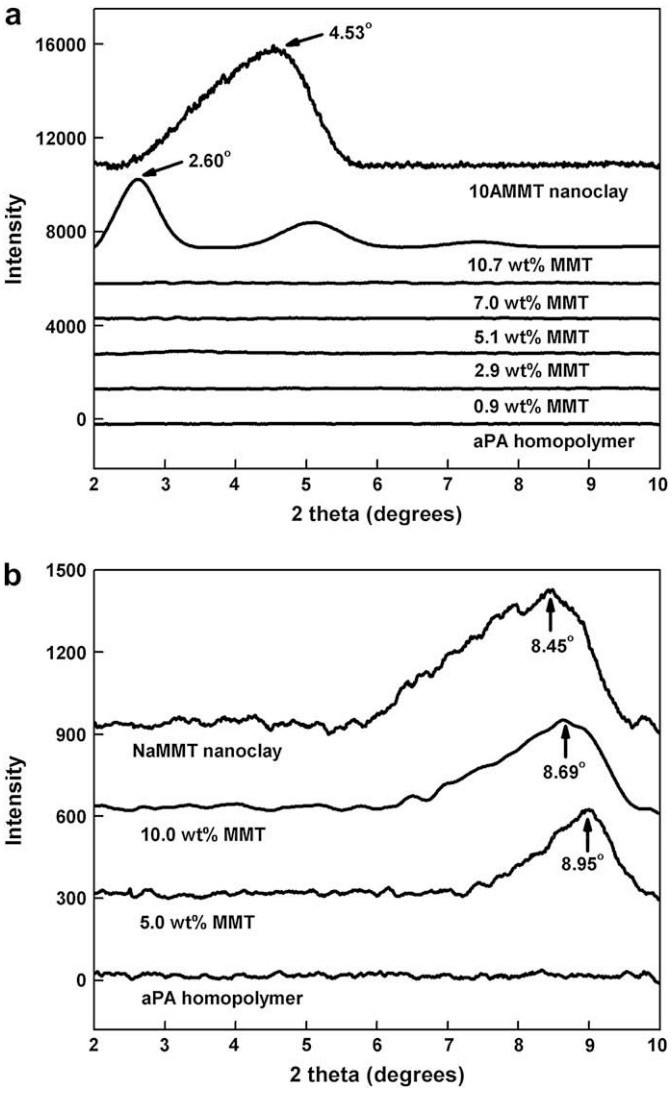

Fig. 2. WAXD patterns for (a) aPA/10AMMT and (b) aPA/NaMMT nanocomposites.

(0.9–7.0 wt% MMT), this basal reflection peak is not observed, suggestive of exfoliated morphology. However, a clear peak at $2\theta = 2.60^\circ$, which corresponds to large d-spacing of 3.38 nm, is observed in aPA/10AMMT containing 10.7 wt% MMT, suggesting the presence of an intercalated structure. Fig. 2b shows the XRD patterns of NaMMT and its nanocomposites. NaMMT powder has a basal peak at $2\theta = 8.45^\circ$ (i.e. d-spacing = 1.05 nm). The NaMMT-based nanocomposites also have the prominent basal peak at the similar values of 2θ, indicating that the clay particles agglomerate in the polymer matrix regardless of the nanoclay concentration.

Fig. 3 shows representative TEM micrographs of these nanocomposite systems. These images support the interpretation of the X-ray results. Fig. 3a shows the TEM image of aPA/10AMMT containing 7.0 wt% MMT. It is observed that the individual clay platelets are randomly but uniformly dispersed within the polymer matrix after the blending and compression molding processes. Similar highly exfoliated nanoclay morphologies are also observed in the TEM micrographs of aPA/10AMMT nanocomposites at low clay loadings (0.9–5.1 wt% MMT). Fig. 3b shows the TEM image of aPA/10AMMT nanocomposite with 10.7 wt% MMT. It reveals the existence of both intercalated and exfoliated structures. The ordered clay arrangement of the intercalated structure gives rise to the XRD peak corresponding to the d-spacing of 3.38 nm seen in Fig. 2a. Fig. 3c shows the TEM image of aPA/NaMMT containing 10.0 wt% MMT. The pristine clay particles agglomerate together and no individual clay platelets are observed. Due to lack of delamination of the nanoclay, the aPA/NaMMT hybrids can be described as traditional microcomposites.

Table 2 lists the molecular weights of the aPA polymer in the nanocomposites as determined by GPC. All the nanocomposites exhibit lower molecular weights than the homopolymer. Furthermore, it is observed that nanocomposites with higher clay content lead to larger reduction in molecular weight of the polymer component. This is consistent with other reports on polymer nanocomposites [48]. Moreover, the level of polymer matrix degradation for the aPA/NaMMT hybrids is more severe than that of the aPA/10AMMT system at similar filler concentration. Isothermal TGA analysis performed on 10AMMT and NaMMT at 270 °C for 10 min in nitrogen showed that 10AMMT has lost greater amount of weight due to decomposition of surfactant [49]. Paul et al. have also shown that the decomposition of surfactant was independent of the decomposition of the polymer [48]. Hence the high degree of polymer degradation observed in polyamide/clay nanocomposites can be attributed largely to the two-step blending process (as opposed to a one-step blending process for the homopolymer) and hydrolysis by interlayer water present in the clay [33,48].

3.2. Thermal analysis

Fig. 4 shows representative TGA and the corresponding differential TGA (DTG) graphs for aPA and its nanocomposites in air. It is observed that the degradation of all the samples occurs in two stages, which is consistent with the results obtained by other researchers for polyamides [22,30]. In the first stage (from 400 °C to 500 °C), the main mass loss occurred in the materials. This is followed by second stage (>500 °C), whereby the char that was formed from the earlier stage experienced continuous oxidative degradation [50]. These two degradation stages gave rise to two DTG peaks in all the samples.

From each TGA/DTG curve, the following data were extracted: (a) $T_{0.05}$, the temperature at which 5 wt% degradation occurred, (b) $T_{0.5}$, the temperature at which 50 wt% degradation occurred, and (c) T_{max1} and T_{max2}, the positions of the two peaks in the DTG curves. $T_{0.05}$ is a measure of the onset temperature of degradation while $T_{0.5}$ is taken to be the midpoint of the degradation process. T_{max1} and

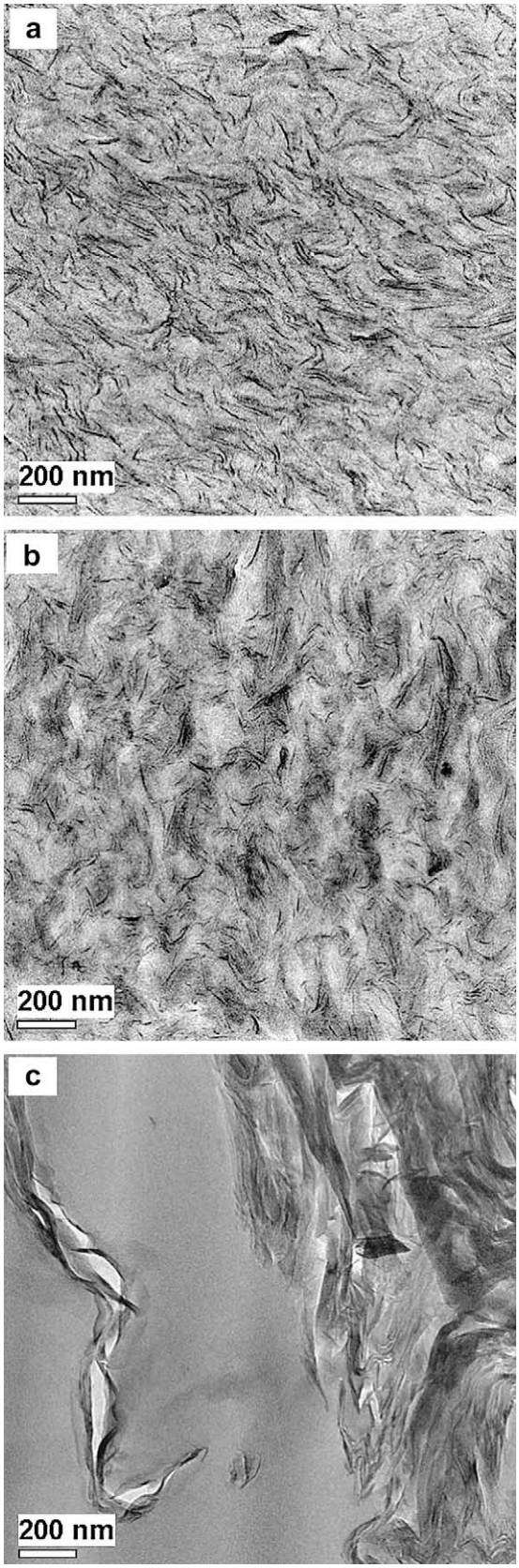

Fig. 3. TEM images of (a) aPA/10AMMT containing 7.0 wt% MMT, (b) aPA/10AMMT containing 10.7 wt% MMT, and (c) aPA/NaMMT containing 10.0 wt% MMT.

Table 2
GPC results for aPA and its nanocomposites.

Samples	M_w (kg/mol)	M_w/M_n
Melt processed aPA	55.8	1.30
aPA/10AMMT[a]		
0.9 wt%	50.4	1.26
2.9 wt%	47.2	1.20
5.1 wt%	48.8	1.33
7.0 wt%	41.6	1.21
10.7 wt%	38.9	1.32
aPA/NaMMT[a]		
5.0 wt%	41.0	1.45
10.0 wt%	31.4	1.30

[a] The clay contents are based on MMT only.

T_{max2} are the temperatures at which the maximum rate of decomposition occurred in the first and second stages, respectively, of the decomposition process. These data are presented in Fig. 5.

Fig. 5a shows the graphs of $T_{0.05}$ and $T_{0.5}$ versus MMT content for the aPA nanocomposites. $T_{0.05}$ of the pure polymer is 400 °C. All nanocomposites containing organoclay 10AMMT have higher $T_{0.05}$ than the neat polymer. Initially $T_{0.05}$ increases with increasing clay content up to a maximum value, it then decreases as clay content increases further. The largest increase was observed in aPA/10AMMT nanocomposites containing 5.1 wt% MMT; this hybrid has a $T_{0.05}$ of 433 °C, a 33 °C increase over that of the homopolymer. This is a significant increase compared to the onset degradation temperature (also under thermo-oxidative conditions) of the nanocomposites based on semicrystalline polyamide 6 or polyamide 66, which showed only an increase of less than 10 °C compared to the respective homopolymers [22,30,51]. Furthermore, TGA studies carried out in a nitrogen atmosphere showed that there was no significant improvement in the thermal stability of aPA/nanoclay nanocomposites compared to the homopolymer [52]. This indicates that the presence of well-dispersed nanoclay effectively enhances the thermal stability of the amorphous polyamide in air but not in nitrogen. For aPA/NaMMT nanocomposite with 5.0% MMT, however, the value of $T_{0.05}$ is only 401 °C, similar to that of aPA. When the MMT content is increased to 10.0 wt% for aPA/NaMMT hybrids, the value of $T_{0.05}$ becomes lower than that of the pure polymer.

The behavior of $T_{0.5}$ versus MMT content is similar to that observed for $T_{0.05}$. $T_{0.5}$ for aPA is 469 °C. For aPA/10AMMT nanocomposites, $T_{0.5}$ increases with increasing clay content up to a maximum of 481 °C for 5.1 wt% MMT (an increase of 12 °C). It then decreases as clay content increases, e.g., $T_{0.5}$ is only 467 °C for 10.7 wt% MMT, similar to that of the pure polymer. The aPA/NaMMT nanocomposites have a $T_{0.5}$ of 476 °C at a clay content of 5.0 wt% MMT, but the value of $T_{0.5}$ drops to 466 °C for 10.0 wt% MMT (lower than that of the homopolymer).

Fig. 5b shows the curves of T_{max1} and T_{max2} versus clay content for the nanocomoposites. The values of T_{max1} and T_{max2} for aPA are 470 °C and 566 °C respectively. For nanocomposites containing 10AMMT organoclay, T_{max1} is higher than that of the homopolymer at all clay contents. Such an increase in the peak mass loss temperature in the DTG curves indicates an inherent stabilizing effect due to the addition of the nanoclay [4,12]. The highest value of T_{max1} is 484 °C for the hybrid with 5.1 wt% MMT (an increase of 14 °C over that of the homopolymer). T_{max1} drops when the MMT content is increased further. T_{max2} for the aPA/10AMMT nanocomposite containing 0.9 wt% clay is similar to that of the pure polymer. However, as clay content increases, T_{max2} increases monotonously with clay content. In contrast, for aPA/NaMMT nanocomposite with 5.0 wt% MMT, there is an increase in T_{max1} but a decrease in T_{max2} compared to aPA. Upon increasing the clay loading to 10.0 wt%, both T_{max1} and T_{max2} drop to values lower than those of the homopolymer.

The TGA results show that there is very little improvement in the thermal stability of melt-blended aPA/NaMMT composites. This behavior is attributed to the limited intercalation of clay layers in these materials as indicated by the TEM and XRD data. On the other hand, the aPA nanocomposites containing organoclay 10AMMT show significant improvement in the ability to withstand thermal oxidation in comparison to the pure polymer. The greatest thermal

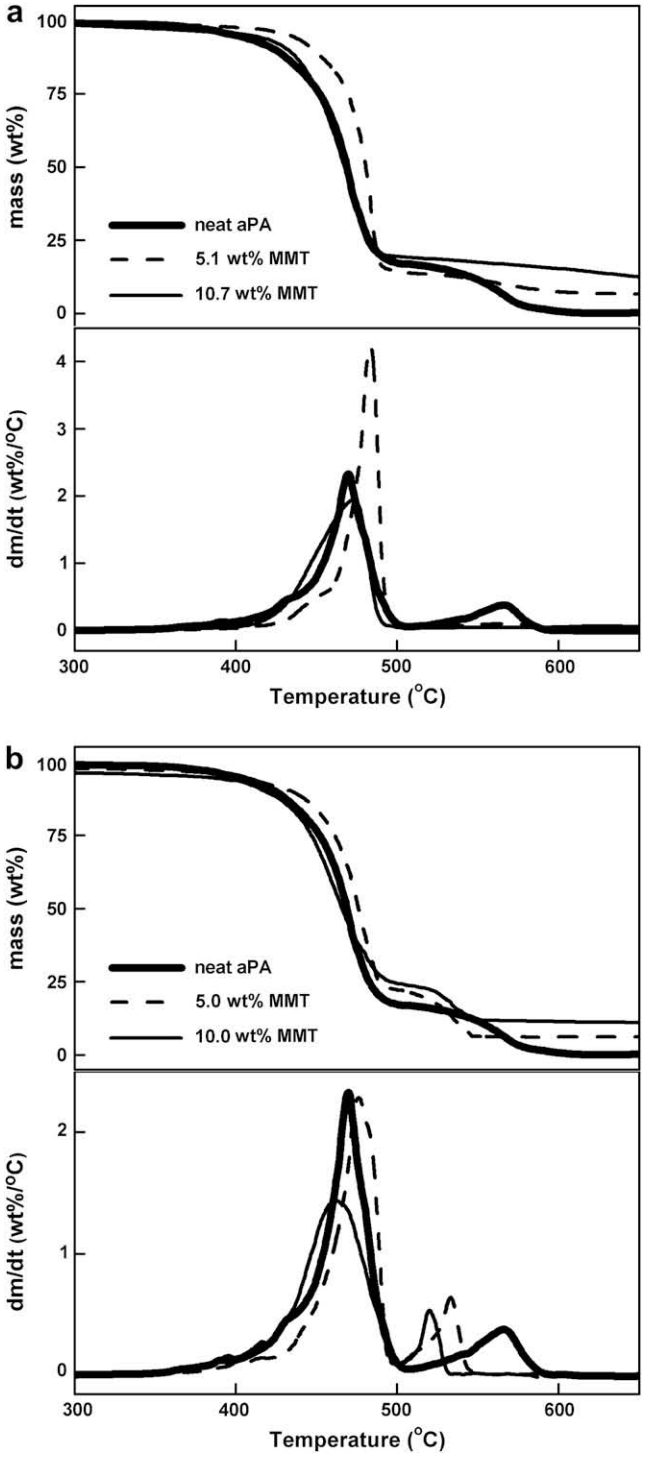

Fig. 4. TGA and DTG curves of (a) aPA/10AMMT and (b) aPA/NaMMT nanocomposites in air with a heating rate of 10 °C/min.

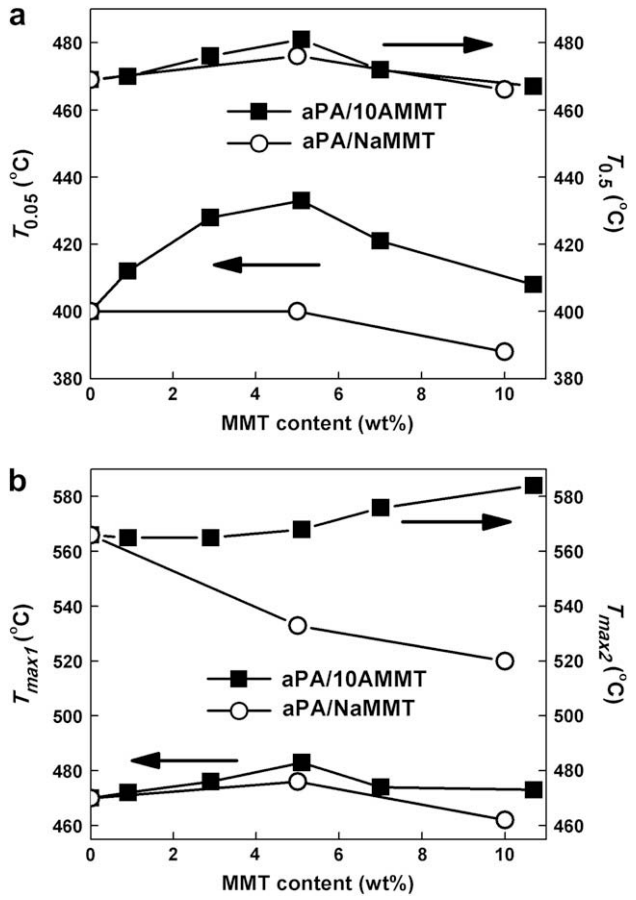

Fig. 5. Effect of clay type and content on (a) $T_{0.05}$ and $T_{0.5}$, (b) T_{max1} and T_{max2} for melt processed aPA and its nanocomposites in air.

stability is obtained for aPA/10AMMT hybrids containing 5.1 wt% MMT. The TGA data for this nanocomposite in air indicate that, at low nanofiller content, there is a significant delay of weight loss that can be attributed to the nanoclay which acts as a impervious barrier retarding the diffusion of the volatile thermo-oxidation products from the polymer bulk to the gas phase as well as retarding the diffusion of oxygen from the gas phase to the polymer bulk [4,18]. However, further increase in the filler content leads to a decrease in thermal properties.

Such a reverse thermal behavior has also been reported for other polymer/nanoclay systems [24,32,53]. According to the proposed barrier model mechanism, at low clay contents, increasing the filler content would lead to increased thermal stability of the nanocomposites. However, at filler content above ca. 5 wt%, complete exfoliation of such high aspect ratio clay layers becomes more hindered because of geometrical constraints within the limited space available in the polymer matrix, hence no further increase in thermal stability can be detected [20]. Such an explanation, however, cannot account for the reverse trend in thermal stability of aPA/10AMMT nanocomposites. This is because the TEM and XRD data have shown that the clay platelets are well-exfoliated up to 7.0 wt% in aPA/10AMMT nanocomposites.

In order to explain this reverse behavior phenomenon, further TGA analysis was carried out for NaMMT and 10AMMT powders. The TGA results are presented in Fig. 6. Fig. 6 shows that the onset of degradation for the pristine clay and organoclay occurred at much lower temperatures (ca. 200 °C) compared to the aPA matrix. Degradation of the organoclay continued up to around 450 °C. These results are consistent with those of Xie et al. who also

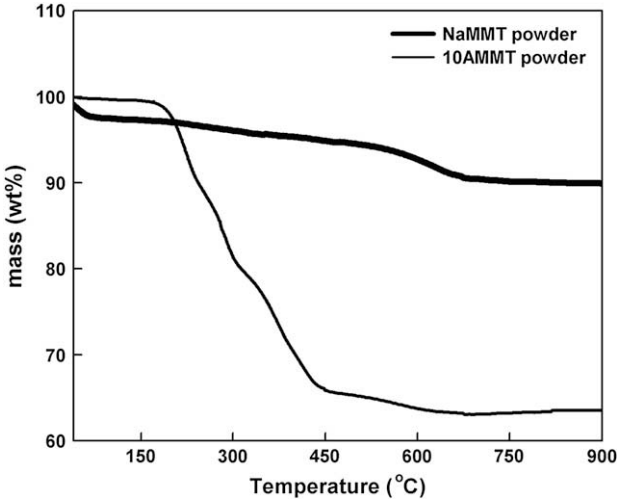

Fig. 6. TGA curves of NaMMT and 10AMMT powder in air with a heating rate of 10 °C/min.

reported that the thermal decomposition of alkyl quaternary ammonium modified MMT occurred mainly in the range from 200 to 500 °C [54]. As clay content increases, the proportion of the surfactants in the polymer nanocomposite also increases. Since the surfactants are less thermally stable than homopolymer aPA, the reverse trend in the thermal stability at high clay contents (>5 wt%) can be attributed partly to the weight loss of the large quantities of surfactants in the polymer nanocomposites.

Molecular weight analysis by GPC (Table 2) also shows that during the blending process, a greater degree of polymer degradation has occurred in nanocomposites containing higher amounts of MMT [33,48]. The increased amount of such chain fragments with lower molecular weight will worsen the thermal stability of the polymer [27,55]. Therefore, in the thermo-oxidative process, the combination of the low onset degradation temperature of the surfactant on the nanoclay, and the increased degree of polymer degradation during melt processing would explain the reverse thermal behavior of aPA/clay nanocomposites.

3.3. Elemental analysis

Table 3 shows the elemental composition of (a) aPA and its nanocomposites containing 5 wt% MMT obtained at room temperature and (b) the residue of aPA and the respective

Table 3
Chemical analysis of aPA and its nanocomposites (containing 5 wt% MMT) obtained after thermal degradation to selected temperatures.

T (°C)	Sample	C (wt%)	H (wt%)	N (wt%)	C:H ratio	C:N ratio
25	aPA (Durethan T40)	67.36	8.10	11.03	8.32	6.11
	aPA/10AMMT	64.10	7.76	10.37	8.26	6.18
	aPA/NaMMT	63.92	7.73	10.39	8.27	6.15
400	aPA (Durethan T40)	67.02	7.77	10.99	8.63	6.10
	aPA/10AMMT	64.15	7.80	10.35	8.22	6.20
	aPA/NaMMT	63.83	7.46	10.22	8.56	6.24
470	aPA (Durethan T40)	78.09	5.84	8.76	13.37	8.91
	aPA/10AMMT	66.14	6.98	9.47	9.47	6.98
	aPA/NaMMT	66.65	6.75	9.64	9.87	6.61
500	aPA (Durethan T40)	80.41	3.34	8.13	24.03	10.59
	aPA/10AMMT	54.70	2.83	5.51	19.33	9.93
	aPA/NaMMT	60.51	2.68	5.94	22.58	10.19
600	aPA (Durethan T40)	0	0	0	–	–
	aPA/10AMMT	13.22	1.69	1.93	7.82	6.85
	aPA/NaMMT	3.72	1.11	0.33	3.35	11.28

nanocomposites after thermal oxidation to the selected temperatures of 400 °C, 470 °C, 500 °C, and 600 °C. For the homopolymer at 25 °C, the composition of the analyzed elements (C, H, and N) is as predicted from its chemical formula. The composition of C, H and N for the polymer nanocomposites at 25 °C is slightly lower than that of the homopolymer because of the presence of the nanoclay. The elemental composition of all the residues obtained at 400 °C does not show any significant changes compared to that at 25 °C. This is consistent with TGA results which indicate only limited degradation at this point.

However, the elemental composition of all the residues obtained at 470 °C shows significant differences compared to those at 25 °C and 400 °C. In pure aPA, there is an increase in the weight percentage of C with a corresponding decrease in the weight percentages of N and H, as indicated by the higher C:N and C:H ratios compared to those at 400 °C. This is indicative of carbonization processes taking place during the first stage of thermal oxidation [56]. The elemental composition of both aPA/nanoclay hybrids also shows larger C:H and C:N ratios at 470 °C than those at lower temperatures, but these ratios are smaller compared to the pure polymer. This implies that the presence of the nanoclay has hindered the thermal oxidation of the polymer matrix.

For the residue obtained at 500 °C, the C:H and C:N ratios of all the samples show a drastic increase compared to those at 470 °C. This is due to the continuous carbonization of the samples. The C:H and C:N ratios for aPA are larger than those for the two polymer nanocomposites, again showing that the carbonization process in air has been retarded by the presence of nanoclay. It is observed that the C:H ratio for the aPA/10AMMT residue (19.33) is smaller than that of both aPA (24.03) and aPA/NaMMT (22.58) residues at 500 °C, indicating that the well-dispersed organoclay in aPA/10AMMT is more effective in retarding the thermal oxidative process.

From TGA results, it is observed that the second stage of thermal oxidation began after 500 °C, at which time the char residue experiences continuous oxidation. From Table 3, for the residue obtained at 600 °C, nothing remained of pure aPA as it has decomposed completely. This is consistent with TGA results for the homopolymer. On the other hand, some organic residue remained for the nanocomposites, indicating that the addition of nanoclay results in the formation of a solid char which has greater thermal stability compared to that of the homopolymer. The higher organic content of the residue of aPA/10AMMT (16.84%) compared to that from aPA/NaMMT (5.16%) shows that the former is more thermally stable [12].

Since all these quantitative differences in the elemental analysis data would necessarily imply some chemical changes in the condensed phase with the addition of nanoclay [24], the FTIR analysis of the solid residue was carried out to elucidate the origin of such changes.

3.4. Infrared spectroscopy

In order to understand the thermal degradation process of aPA and its clay hybrids in air, FTIR spectra were obtained for the residue which had been subjected to thermal degradation up to the selected temperatures of 350 °C, 400 °C, 430 °C, 450 °C, 470 °C, 480 °C, and 500 °C.

3.4.1. Infrared spectra of pure aPA

Figs. 7 and 8a show the infrared spectra (in the range 4000–400 cm^{-1} and 660–600 cm^{-1} respectively) of aPA at room temperature as well as those of the residue obtained at higher temperatures. Baseline correction has been applied to all spectra. Table 4 lists the main FTIR band assignments for aPA at room temperature [36,57]. In the following discussion for the homopolymer, we will examine some key infrared bands and trace their evolution through the residue obtained at different temperatures.

3.4.1.1. NH stretching, Amide I, Amide II and aliphatic CH_2 stretching bands. In Fig. 7, it is observed that the main structural features of aPA seen in the infrared spectrum at 25 °C are still present in the spectra of the residue obtained at 350 °C and 400 °C. The NH stretching (3310 cm^{-1}), Amide I (1642 cm^{-1}), Amide II (1541 cm^{-1}) and CH_2 stretching (2932 cm^{-1} and 2858 cm^{-1}) peaks remain fairly sharp and distinct. Drastic changes to these peaks are first observed in the infrared spectra of the residue at 430 °C and 450 °C. First, the relative intensities of these bands are greatly diminished. Second, the Amide I and Amide II peaks are becoming less sharp and less distinct. In the infrared spectra of the residue at 470 °C and higher temperatures, all the amide related peaks and aliphatic CH_2 stretching peaks have virtually disappeared.

3.4.1.2. Free C═O stretching band (1720 cm^{-1}). In Fig. 7, this peak is present in the pure polymer at 25 °C and persists in the infrared spectra of the residue up to 500 °C. In order to trace the evolution of the free C═O peak in the residue at different temperatures, the ratio (I_1) of the peak height of the 1720 cm^{-1} band to peak height of the Amide I band at 1642 cm^{-1} was determined. A flat baseline was drawn from 1850 to 850 cm^{-1} for each spectrum to obtain the corresponding peak heights. The results are shown in Table 5. The values of I_1 were only determined up to 450 °C because at higher temperatures the peak at 1720 cm^{-1} becomes a shoulder and it is no longer possible to obtain its height accurately (Fig. 7).

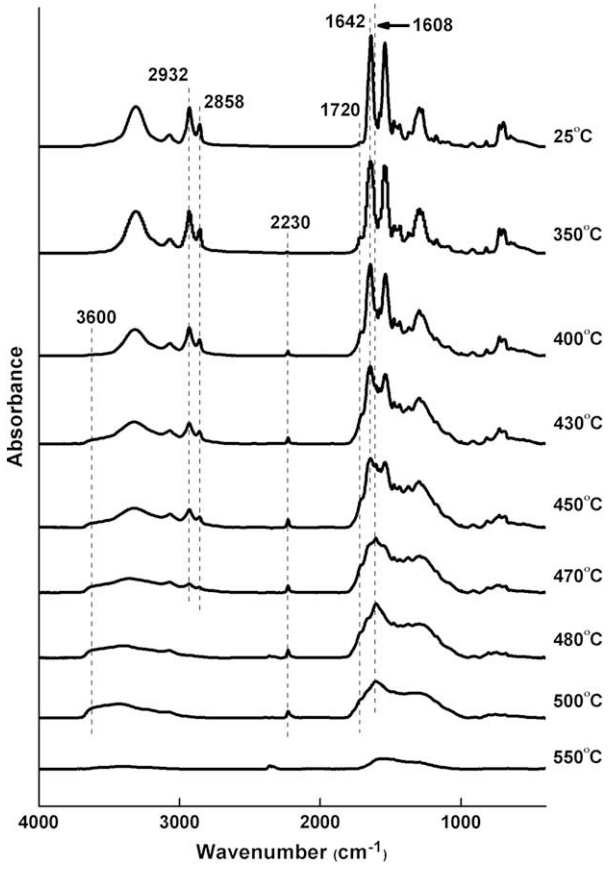

Fig. 7. FTIR spectra of pure aPA at 25 °C and its solid residue obtained at selected temperatures of 350 °C, 400 °C, 430 °C, 450 °C, 470 °C, 480 °C, 500 °C and 550 °C.

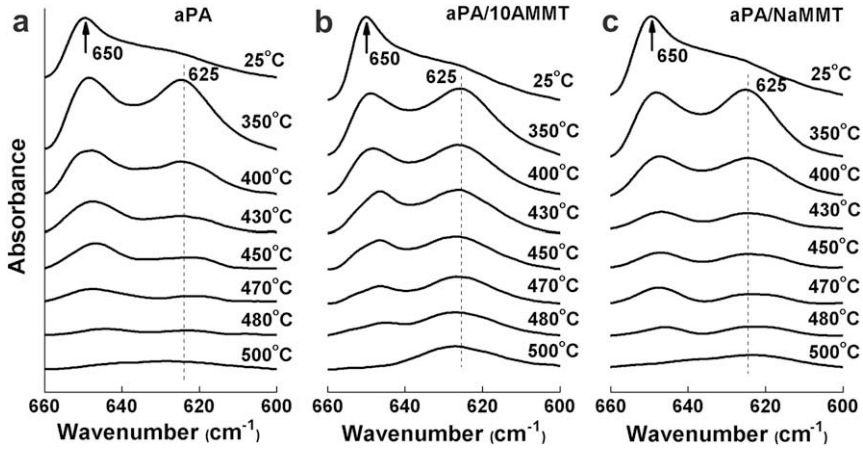

Fig. 8. FTIR spectra in the region of 660–600 cm^{-1} of (a) aPA, (b) aPA/10AMMT with 5.1 wt% MMT, (c) aPA/NaMMT with 5.0 wt% MMT residue at selected temperatures.

The second column in Table 5 shows the ratios for aPA and its residue. The ratio I_1 increases by a factor of 4 from 25 °C to 350 °C, and continues to increase even for the residue at 400 °C and 430 °C. This indicates a monotonous increase in the relative intensity of the free carbonyl band with increasing temperature of thermal oxidation.

3.4.1.3. Aromatic C═C stretch band at 1608 cm^{-1}. In Fig. 7, this peak is ascribed to C═C skeletal vibrations in aromatic groups. It is also present in the FTIR spectrum of the polymer at 25 °C. The ratio, I_2, of the peak height of the 1608 cm^{-1} peak to that of the Amide I band at 1642 cm^{-1} was determined and shown in the third column of Table 5. From 25 °C to 350 °C, there is an increase in I_2 by 50%, and this ratio continues to increase for the residue up to 450 °C. At 470 °C, the 1608 cm^{-1} peak becomes dominant as the Amide I and Amide II bands are reduced to shoulders. The 1608 cm^{-1} peak also persists with increasing heat-treated temperature up to 500 °C.

3.4.1.4. Appearance of new peak at 2230 cm^{-1}. In Fig. 7, this peak is absent in the FTIR spectrum of the polymer at 25 °C and first appears in the spectrum of the residue at 350 °C. This peak is attributed to the presence of aryl nitrile bonds (C≡N stretch) [59]. It is also present in all the spectra of the residue from 400 °C to 500 °C.

3.4.1.5. Appearance of new peak at 625 cm^{-1}. In Fig. 8a, this peak is absent in the FTIR spectrum of the polymer at 25 °C and first appears as a distinct peak in the spectrum of the residue at 350 °C. This particular absorption originates from the presence of terminal vinyl groups (*cis*-CH in-phase wag) in the residue [60]. In the infrared spectrum of the residue at 350 °C, the peak height is larger than that of the N–C═O bending peak at 650 cm^{-1}. However, in the spectra of the residue from 400 °C to 450 °C, it is observed that the intensity of the 625 cm^{-1} peak is lower than that of the 650 cm^{-1} peak. Furthermore, both peaks become greatly diminished in intensity in the residue above 450 °C.

3.4.1.6. Appearance of new peak in the region of 3500–3650 cm^{-1}. In Fig. 7, this peak is absent in the FTIR spectrum of the polymer at 25 °C and first appears as a broad band in the spectrum of the residue obtained at 400 °C. This band is attributed to the presence of hydroxyl-containing single groups [61]. It persists in all the spectra of the residue from 400 °C to 500 °C.

3.4.1.7. Proposed mechanisms of thermal decomposition for aPA. There are a couple of pathways through which pure aPA can decompose [62]. Ballistreri et al. proposed a mechanism for the thermal degradation of aPA in the absence of oxygen up to 380 °C. The reaction is shown in Scheme 1. The first step (Step 1 in Scheme 1) involves chain fragmentation in the homopolymer via a β-CH hydrogen transfer process resulting in products containing olefinic and amide end-groups. The products which contain the amide end-groups can then undergo further thermal decomposition to form compounds with aryl nitrile end-groups (Step 2 in Scheme 1).

On the other hand, aPA can also decompose via an alternate pathway in the presence of oxygen as shown in Scheme 2, which is based on the thermo-oxidative pathway of aliphatic polyamides as proposed by Do et al. [63]. In Step 1, thermal oxidation is initiated by the abstraction of a hydrogen atom from an *N*-vicinal methylene group. In the propagating step (Step 2 in Scheme 2), the free radicals formed in Step 1 are oxidized to produce the unstable *N*-acylamide structure and free OH group respectively. Subsequently, the *N*-acylamide group can decompose to produce species

Table 4
FTIR band assignments of aPA at room temperature.

Wavenumber (cm^{-1})	Band assignment
3310	Hydrogen-bonded N–H stretch
3069	Aromatic C–H stretch, and Fermi-resonance of NH stretching with the overtone of Amide II
2932	Asymmetric CH_2 stretch
2858	Symmetric CH_2 stretch
1720	Free C═O stretch [58]
1642	Amide I mode
1608	Aromatic C═C stretch [56]
1541	Amide II mode
1299	Amide III mode
700	Amide V mode
650	N–C═O in-plane bend [59]

Table 5
FTIR band intensity ratio, $I_1 = I_{1720}/I_{1642}$, and $I_2 = I_{1608}/I_{1642}$ of aPA, aPA/10AMMT and aPA/NaMMT as well as their residue obtained at various temperatures.

	aPA		aPA/10AMMT hybrid		aPA/NaMMT hybrid	
T (°C)	I_1	I_2	I_1	I_2	I_1	I_2
25	0.043	0.241	0.042	0.240	0.042	0.240
350	0.179	0.371	0.120	0.293	0.156	0.340
400	0.259	0.503	0.175	0.411	0.226	0.456
430	0.376	0.754	0.189	0.495	0.251	0.670
450	None[a]	0.917	0.203	0.548	None[a]	0.891

[a] The exact peak height cannot be obtained because the 1720 cm^{-1} band appears as a shoulder at this temperature.

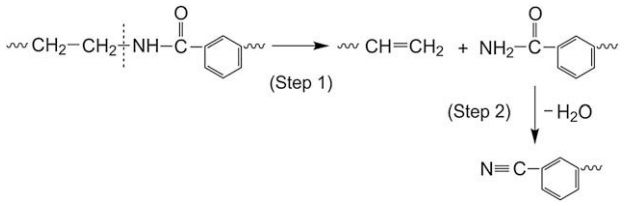

Scheme 1. The thermal degradation mechanism of aPA in the absence of oxygen [62].

containing cyano and acid groups (Step 3 in Scheme 2) [63,64]. Further oxidation of these species can occur via hydrogen elimination and polycondensation reactions resulting in a residue with increasing degree of aromaticity (Step 4 in Scheme 2) [26].

The FTIR and EA data of the aPA residue allow us to conclude that both mechanisms shown in Schemes 1 and 2 have taken place in the thermal decomposition of homopolymer aPA in air. In the residue obtained at 350 °C, the appearance of the terminal vinyl absorption band at 625 cm^{-1} (Fig. 8a) is consistent with the products of thermal degradation in the absence of oxygen as shown in Scheme 1. At the same time, the observed increase in the ratio I_1 at 350 °C in the second column of Table 5 indicates that aPA chains also undergo thermal degradation as depicted in Scheme 2, since this would lead to products containing more C=O groups. It is also to be noted that both Schemes 1 and 2 produce species containing aryl nitrile (C≡N) groups. Hence we can conclude that at this stage, i.e. 350 °C, both oxidative and non-oxidative thermal degradation processes are already taking place in the polymer.

This shows that the FTIR analysis of the residue is a sensitive technique because the data from bulk techniques such as TGA ($T_{0.05}$ in Fig. 5a) did not show any significant changes in the mass loss or chemical composition of the polymer at 350 °C. Based on these data, we further propose that the initial decomposition process occurs only in a very thin "skin" layer on the surface of the polymer. In fact the oxidative process would occur in the outer part of "skin" region which is exposed to oxygen while the non-oxidative process takes place in the inner part of the "skin" region where oxygen has not diffused to.

Furthermore, based on the FTIR data of Fig. 7, for Scheme 2 Step 3, of the two C–N bonds in the *N*-acylamide group, only the C–N bond adjacent to the methylene group was broken in the degradation process leading to the formation of products containing the aryl nitrile group. If the C–N bond adjacent to the phenyl ring was also broken, it would lead to products containing alkyl nitrile groups which would have an FTIR band at 2250 cm^{-1} [24]. Such a peak, however, was not observed. Only the aryl nitrile band at 2230 cm^{-1} has been observed in Fig. 7. This is reasonable as the aryl nitrile group is more stable than the alkyl nitrile group since the former is stabilized by resonance effects through the phenyl ring.

For thermal oxidation processes, the degree of oxidation can be estimated by the concentration of oxidized groups such as the carbonyl band at 1720 cm^{-1} and the broad band due to hydroxyl groups at 3500–3650 cm^{-1} [61,65]. As temperature increases to 400 °C, the degradation process occurs more dominantly via the oxidative reaction of Scheme 2 and less of aPA decomposes via Scheme 1. This conclusion is substantiated by the increase in the ratio I_1 in Table 5 and by the simultaneous decrease in peak height of the terminal vinyl peak at 625 cm^{-1} relative to the 650 cm^{-1} peak (Fig. 8a). At the same time, the appearance of the broad peak in the region of 3500–3650 cm^{-1} at 400 °C in Fig. 7 indicates the presence of accumulated free hydroxyl groups, consistent with degraded products according to Scheme 2. At 400 °C, since $T_{0.05}$ for aPA has been reached (Fig. 5a), this indicates that the degradation has progressed somewhat beyond the initial "skin" region. The dominance of the oxidative reaction is attributed to the diffusion of oxygen into the inner regions of the polymer. The non-oxidative reaction continues to occur in the region of the polymer where oxygen has not diffused to. The loss of hydrogen atoms from CH_2 and NH groups, as depicted in Schemes 1 and 2, is also reflected in the EA and FTIR data. EA results in Table 3 show a slight increase in the C:H ratio at 400 °C compared to that at 25 °C. The FTIR spectra in Fig. 7 shows a slight decrease in the intensity of the NH stretch band (3310 cm^{-1}) and aliphatic CH_2 stretch bands (2932 cm^{-1} and 2858 cm^{-1}) at 400 °C compared to 25 °C. These results further confirm the validity of the thermal decomposition pathways for aPA proposed by Schemes 1 and 2.

As temperature increases, the oxidative reaction of Scheme 2 continues to dominate the degradation process, as indicated by the continued decrease in relative intensity of the 625 cm^{-1} peak (Fig. 8a) and by the increase in the ratio I_1. The prevalence of carbonyl and hydroxyl groups is consistent with oxidative reactions of organic polymers.

Subsequently, as seen in Fig. 7, the peak intensities of all the amide bands are drastically diminished between 450 °C and 470 °C, and the aliphatic CH_2 stretch peaks almost disappear at 480 °C. In contrast, the aromatic C=C band centered at 1608 cm^{-1} persists even up to 500 °C. These imply the increasing aromaticity of the materials as hydrogen elimination and polycondensation reactions take place (Step 4 in Scheme 2) [26]. This is also consistent with EA data which shows a large increase in C content and a large decrease in H and N components at 470 °C and 500 °C.

As temperature increases from 500 °C to 600 °C, the main reactions taking place are continuous oxidation of carbon residue. In Fig. 7, at 550 °C, the fairly featureless FTIR spectrum of the sample is typical of amorphous carbonaceous materials [56].

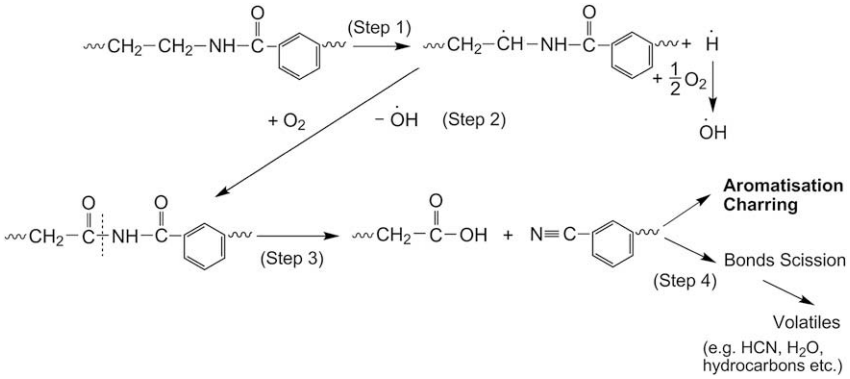

Scheme 2. Thermal degradation mechanism of aPA in the presence of oxygen (the intermediates as drawn do not imply a concerted mechanism, but show the possible rearrangement of atoms and bonds) [63,64].

3.4.2. Infrared spectra of aPA/10AMMT nanocomposite and its residue

Figs. 9 and 8b show the infrared spectra (in the range 4000–400 cm^{-1} and 660–600 cm^{-1} respectively) of aPA/10AMMT with 5.1 wt% MMT at room temperature as well as those of the residue obtained at higher temperatures. At room temperature, the FTIR spectrum of the polymer nanocomposite is similar to that of aPA, except for the additional MMT bands at 3627 cm^{-1}, 1045 cm^{-1}, 520 cm^{-1} and 462 cm^{-1} which are attributed to the bonded hydroxyl stretch, Si–O stretch, Si–O–Al^{3+} deformation and Si–O–Si deformation respectively [66,67].

In Fig. 9, it is observed that the NH stretching, Amide I, Amide II and CH_2 stretching peaks remain very sharp and distinct even up to 470 °C. This is in contrast to the spectra for aPA where drastic changes to these peaks are first observed at 430 °C. In the nanocomposite, the intensities of these 5 peaks are observed to be greatly diminished only in the spectrum at 480 °C and they virtually disappear in the spectrum only at 500 °C.

The ratio (I_1) of the peak height of the free C═O stretching band at 1720 cm^{-1} to the peak height of the Amide I band at 1642 cm^{-1} was determined and tabulated in the fourth column of Table 5. It is observed that I_1 shows a monotonous increase from 25 °C up to 450 °C. At 25 °C, the ratio I_1 for aPA/10AMMT is similar to that of aPA but at higher temperatures, the values of I_1 are significantly lower than aPA, indicating a lower degree of oxidation in the polymer nanocomposite.

The aromatic C═C stretch band at 1608 cm^{-1} is present at 25 °C and becomes dominant at 500 °C. The ratio, I_2, of the peak height of the 1608 cm^{-1} peak to that of the Amide I band at 1642 cm^{-1} was determined and shown in the fifth column of Table 5. It is observed that I_2 increases monotonously with temperature but the values of I_2 are lower for the nanocomposite than the pure polymer at high temperatures.

In Fig. 8b, the peak at 625 cm^{-1} arising from terminal vinyl groups of the aPA nanocomposite first appears in the spectrum of the residue at 350 °C. From 350 °C to 500 °C, the relative intensity of this peak is always higher than that of the N–C═O bending band at 650 cm^{-1}. This behavior is opposite to that for pure aPA, in which the intensity of the 625 cm^{-1} peak is smaller than that of the 650 cm^{-1} peak at all temperatures except 350 °C. Furthermore, in aPA, both peaks become greatly diminished in intensity in the residue at higher temperatures while in the nanocomposite, the peak at 625 cm^{-1} still shows very strong absorption even up to 500 °C.

Table 6 summarizes the key differences in the FTIR spectra of aPA and aPA/10AMMT nanocomposites.

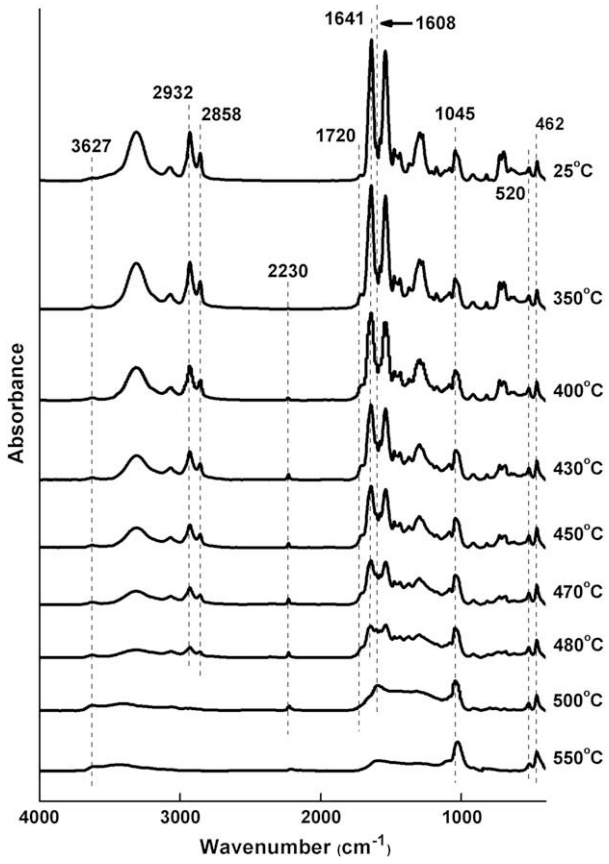

Fig. 9. FTIR spectra of aPA/10AMMT with 5.1 wt% MMT and its solid decomposition products at selected temperatures.

3.4.3. Infrared spectra of aPA/NaMMT nanocomposite and its residue

Fig. 10 shows the infrared spectra (in the range 4000–400 cm^{-1}) of aPA/NaMMT with 5.0 wt% MMT at room temperature as well as those of the residue obtained at higher temperatures. The room temperature FTIR spectrum of aPA/NaMMT shows all the characteristic bands of aPA and nanoclay, similar to that of aPA/10AMMT. Table 6 summarizes the key differences between the FTIR of aPA/NaMMT and the other two systems.

On close examination of Figs. 7, 9 and 10, it can be seen that the changes taking place in the chemical structure of the residue of aPA/NaMMT is intermediate between that of the homopolymer and that of the aPA/10AMMT nanocomposite. Similarly, the values of I_1 and I_2 as presented in the sixth and seventh columns of Table 5 for aPA/NaMMT and its residue are also intermediate between aPA and aPA/10AMMT. In Fig. 10, the characteristic broad absorption of free hydroxyl groups first appears at 430 °C for aPA/NaMMT. This is a lower temperature compared to that for aPA/10AMMT residue (450 °C). The dominance of the C═C band at 1608 cm^{-1} over the Amide I and Amide II peaks also occurs at a lower temperature (480 °C) than that of aPA/10AMMT (500 °C).

Fig. 8c shows the FTIR spectra of aPA/NaMMT hybrid at room temperature as well as those of the residue obtained at higher temperatures in the region of 660–600 cm^{-1}. The 625 cm^{-1} peak due to terminal vinyl groups first appears in the spectrum of the residue at 350 °C. Though the intensity of this peak is higher than the 650 cm^{-1} peak at 350 °C, its intensity is generally lower than the latter at higher temperatures. This is similar to the trend seen for pure aPA.

3.4.4. Proposed thermal decomposition mechanisms for aPA matrix in the presence of nanoclay

The decomposition mechanism of aPA in the aPA/nanoclay nanocomposites is proposed in light of FTIR and EA data of the residue.

3.4.4.1. aPA/10AMMT. The appearance of the terminal vinyl absorption at 625 cm^{-1} (Fig. 8b) and the relative increase in the band intensity of free C═O stretch at 1720 cm^{-1} (Table 5) both occurred at 350 °C. Hence it indicates that at this stage, the aPA matrix in the nanocomposites also experienced both non-oxidative and oxidative thermal degradation as shown in Schemes 1 and 2. This is very similar to aPA. The initial decomposition is also postulated to occur in a very thin "skin" layer on the surface of the polymer nanocomposite.

As temperature increases to 400 °C, it is clear that the non-oxidative Scheme 1 plays a more important role in the thermal decomposition of the aPA/10AMMT nanocomposite than for the homopolymer. This is because the relative intensity of the terminal vinyl peak at 625 cm^{-1} increases for the nanocomposite in Fig. 8b,

Table 6
Summary of key differences in the FTIR spectra of aPA, aPA/10AMMT and aPA/NaMMT.

FTIR bands	aPA	aPA/10AMMT nanocomposite	aPA/NaMMT nanocomposite
NH stretching, Amide I, Amide II and aliphatic CH_2 stretching bands	Greatly diminished at 430 °C Disappeared at 470 °C	Greatly diminished at 480 °C Disappeared at 500 °C	Greatly diminished at 430 °C Disappeared at 470 °C
Free C═O stretching band (1720 cm^{-1})	Highest values of I_1 (Table 5)	Lowest values of I_1 (Table 5)	Intermediate values of I_1 (Table 5)
Aromatic C═C stretch band at 1608 cm^{-1}	Highest values of I_2 (Table 5)	Lowest values of I_2 (Table 5)	Intermediate values of I_2 (Table 5)
Terminal vinyl groups (*cis*-CH in-phase wag) at 625 cm^{-1}	Peak height of 625 cm^{-1} peak smaller than that of 650 cm^{-1} peak at all temperatures larger than 350 °C Greatly diminished at high temperatures	Peak height of 625 cm^{-1} peak larger than that of 650 cm^{-1} peak at all temperatures larger than 350 °C Very strong absorption even at high temperatures	Peak height of 625 cm^{-1} peak smaller than that of 650 cm^{-1} peak at all temperatures larger than 350 °C Greatly diminished at high temperatures
Hydroxyl-containing single groups at 3500–3650 cm^{-1}	First appeared at 400 °C	First appeared at 450 °C	First appeared at 430 °C

while that of the homopolymer decreases in Fig. 8a. At this temperature, $T_{0.05}$ for aPA/10AMMT has not been reached yet (its $T_{0.05}$ is 433 °C). Since very little amount of decomposition has occurred at this stage for the polymer nanocomposite, the loss of hydrogen atoms from CH_2 and NH groups could not be observed from the EA data in Table 3 and FTIR spectra in Fig. 9 respectively. However, for the homopolymer, the changes in the chemical composition were already evident.

As temperature increases from 400 °C to 500 °C, the degradation of aPA in aPA/10AMMT nanocomposite continues to occur via both Schemes 1 and 2. The non-oxidative Scheme 1 continues to play an important role in the degradation process as compared to for the homopolymer. This is confirmed by higher relative intensity of the 625 cm^{-1} peak compared to the 650 cm^{-1} peak in Fig. 8b. As mentioned before, for polymer thermo-oxidative study, the extent of oxidation can be characterized by the increased band intensity of free C═O stretch and the accumulation of free OH groups. From Table 5, it is observed that the increase in the ratio I_1 for the residue of aPA/10AMMT is significantly less than that for the residue of pure aPA. Furthermore, the appearance of the free OH stretching absorption in the range of 3500–3650 cm^{-1} occurs at a higher temperature (450 °C) for aPA/10MMT compared to that of the homopolymer residue (400 °C). The relatively low concentrations of both free hydroxyl species and free carbonyl groups indicate that the addition of well-dispersed nanoclay dramatically retards the thermal oxidation of aPA matrix.

Moreover, in Fig. 9, it is seen that all the amide related bands in the FTIR spectra have become less sharp and less distinctive at 480 °C. Subsequently, the aromatic C═C stretch band at 1608 cm^{-1} becomes dominant at 500 °C. These indicate the retardation of polycondensation reactions in the aPA/10AMMT nanocomposite. The protective effect is also confirmed by the existence of strong aliphatic CH_2 stretch bands (2932 and 2858 cm^{-1}) above 480 °C in the nanocomposite, while in the pure polymer they have virtually disappeared at 470 °C.

Above 500 °C, the residue of aPA/10AMMT also underwent continuous thermal oxidation, as indicated by their FTIR spectra at 550 °C which shows the similar absorption bands of amorphous carbonaceous materials as that of aPA residue at the same temperature. Besides the inorganic residue from the clay fillers, a substantial amount of organic residue still remained for the nanocomposites at 600 °C as observed from EA data. However, no residue remained for the homopolymer at 600 °C.

In summary, these results show that the presence of well-dispersed organoclay 10AMMT has greatly influenced the degradation pathway of aPA matrix. The delaminated clay layers serve to restrict the thermal motion of the polymer segments [15,16,68] and to retard the permeation rate of air through the polymer [69]. Consequently, the non-oxidative Scheme 1 became a more significant mechanism through which these constrained polymer chains would degrade. However, the delaminated nanoclay is not as effective in retarding the non-oxidative reaction process for this polymer. This could explain why the results of polymer degradation performed under inert atmosphere do not show dramatic improvements in the thermal stability for some polymer/nanoclay nanocomposites [22,24,26].

3.4.4.2. aPA/NaMMT. At 350 °C, the appearance of the terminal vinyl absorption at 625 cm^{-1} (Fig. 8c) and the relative increase in the band intensity of free C═O stretch at 1720 cm^{-1} (Table 5)

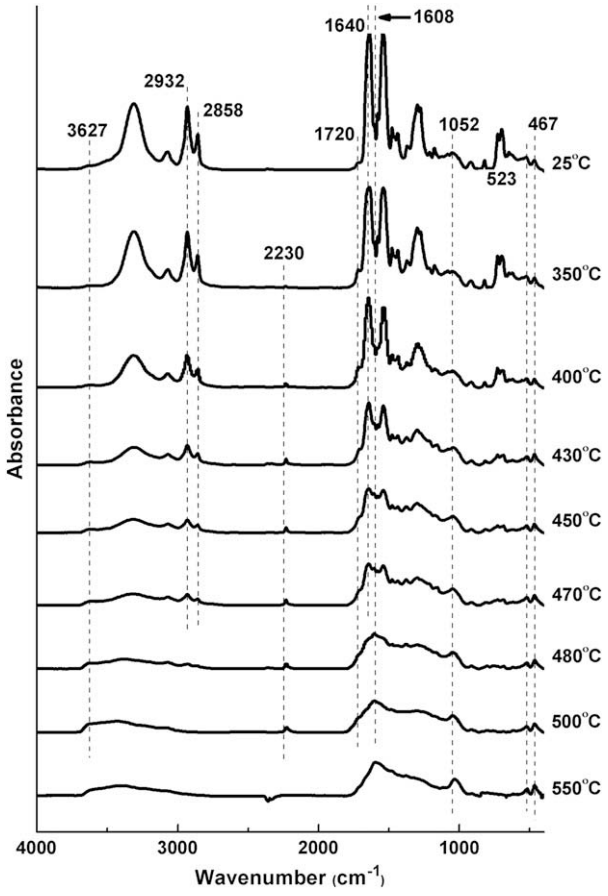

Fig. 10. FTIR spectra of aPA/NaMMT with 5.0 wt% MMT and its solid decomposition products at selected temperatures.

shows that aPA/NaMMT also degraded via both Schemes 1 and 2. In Fig. 8c, the lower peak height of the 625 cm^{-1} peak relative to the 650 cm^{-1} peak at higher temperatures indicates that Scheme 2 plays a more important role in the thermal decomposition of the aPA/NaMMT, just like the homopolymer. This is in contrast to the scenario for aPA/10AMMT. The TGA, EA and FTIR results show that the presence of aggregated NaMMT delays the oxidation rate of aPA matrix to a lesser extent compared to well-dispersed nanoclay. As the barrier effect is not as significant in this aggregated system, so the limited improvement in thermal oxidative stability is attributed to the promotion of char formation in the polymer matrix during the degradation process [11,12,26].

4. Conclusion

A novel aPA/MMT nanocomposite formed by melt processing is presented in this study. The presence of a surfactant on montmorillonite leads to well-exfoliated nanoclay morphology and improved thermal oxidative stability at filler content of up to 5%. In this hybrid system, the reverse behavior of thermal stability observed at higher nanoclay content is attributed to the low onset degradation temperature of the surfactant on the nanoclay and the increased degree of polymer degradation caused by melt processing. Inorganic clay without surfactant tends to agglomerate in the polymer matrix, and the resulting system does not have a similar degree of oxidation stability as the organoclay nanocomposite.

FTIR and elemental analysis of the thermal decomposition residue have been proven to be very useful for providing informative data on the mechanisms of the degradation process in air. From elemental analysis, some quantitative differences are observed between the pure polymer and its nanocomposites, indicating that the presence of nanoclay leads to char formation with greater thermal stability. FTIR spectra of the condensed phase reveal the possible decomposition pathways of aPA matrix and the relative dominance of each pathway. It shows that nanoclay dramatically hinders the polymer oxidative process. From the viewpoint of barrier effect, the well-dispersed nanoclay layers shield the polymer from the action of oxygen, hence the degradation process of constrained aPA segments has been influenced. This demonstrates that FTIR and elemental analysis on the condensed phase can complement TGA/FTIR and GC/MS analysis of the evolved phase to reveal the possible decomposition mechanisms of polymer nanocomposite systems.

Acknowledgment

The work was sponsored by a grant from Nanyang Technological University. The authors thank Prof. Mary Chan and Ms. Ruoshan Tan for the use of their materials and equipment.

References

[1] Usuki A, Koiwai A, Kojima Y, Kawasumi M, Okada A, Kurauchi T, et al. J Appl Polym Sci 1995;55(1):119–23.
[2] Kawasumi M, Hasegawa N, Kato M, Usuki A, Okada A. Macromolecules 1997;30(20):6333–8.
[3] Vaia RA, Giannelis EP. Macromolecules 1997;30(25):7990–9.
[4] Gilman JW, Jackson CL, Morgan AB, Harris R, Manias E, Giannelis EP, et al. Chem Mater 2000;12(7):1866–73.
[5] Fornes TD, Paul DR. Macromolecules 2004;37(20):7698–709.
[6] Kojima Y, Usuki A, Kawasumi M, Okada A, Kurauchi T, Kamigaito O. J Polym Sci Part A Polym Chem 1993;31(7):1755–8.
[7] Usuki A, Kojima Y, Kawasumi M, Okada A, Fukushima Y, Kurauchi T, et al. J Mater Res 1993;8(5):1179–84.
[8] Fornes TD, Yoon PJ, Keskkula H, Paul DR. Polymer 2001;42(25):9929–40.
[9] Gilman JW. Appl Clay Sci 1999;15(1–2):31–49.
[10] Zhu J, Uhl FM, Morgan AB, Wilkie CA. Chem Mater 2001;13(12):4649–54.
[11] Zhu J, Morgan AB, Lamelas FJ, Wilkie CA. Chem Mater 2001;13(10):3774–80.
[12] Gilman JW, Harris RH, Shields JR, Kashiwagi T, Morgan AB. Polym Adv Technol 2006;17(4):263–71.
[13] Blumstein A. J Polym Sci 1965;3(7):2665–72.
[14] Vyazovkin S, Dranca I, Fan X, Advincula R. J Phys Chem B 2004;108(31):11672–9.
[15] Pinnavaia TJ, Beall GW. Polymer–clay nanocomposites. New York: Wiley; 2000.
[16] Chen K, Wilkie CA, Vyazovkin S. J Phys Chem B 2007;111(44):12685–92.
[17] Xie W, Gao ZM, Liu KL, Pan WP, Vaia R, Hunter D, et al. Thermochim Acta 2001;367:339–50.
[18] Zanetti M, Kashiwagi T, Falqui L, Camino G. Chem Mater 2002;14(2):881–7.
[19] Qiu LZ, Chen W, Qu BJ. Polymer 2006;47(3):922–30.
[20] Leszczynska A, Njuguna J, Pielichowski K, Banerjee JR. Thermochim Acta 2007;453(2):75–96.
[21] Kashiwagi T, Harris RH, Zhang X, Briber RM, Cipriano BH, Raghavan SR, et al. Polymer 2004;45(3):881–91.
[22] Qin HL, Su QS, Zhang SM, Zhao B, Yang MS. Polymer 2003;44(24):7533–8.
[23] Leswzynska A, Njuguna J, Pielichowski K, Banerjee JR. Thermochim Acta 2007;454(1):1–22.
[24] Jang BN, Wilkie CA. Polymer 2005;46(10):3264–74.
[25] Chiu FC, Lai SM, Chen YL, Lee TH. Polymer 2005;46(25):11600–9.
[26] Zanetti M, Bracco P, Costa L. Polym Degrad Stab 2004;85(1):657–65.
[27] Krzysztof P, Njuguna J. Thermal degradation of polymeric materials. Shrewsbury: Rapra Technology; 2005.
[28] Jang BN, Wilkie CA. Polymer 2005;46(23):9702–13.
[29] Bourbigot S, Le Bras M, Dabrowski F, Gilman JW, Kashiwagi T. Fire Mater 2000;24(4):201–8.
[30] Pramoda KP, Liu TX, Liu ZH, He CB, Sue HJ. Polym Degrad Stab 2003;81(1):47–56.
[31] Chen K, Vyazovkin S. Macromol Chem Phys 2006;207(6):587–95.
[32] Liu TX, Lim KP, Tjiu WC, Pramoda KP, Chen ZK. Polymer 2003;44(12):3529–35.
[33] Davis RD, Gilman JW, VanderHart DL. Polym Degrad Stab 2003;79(1):111–21.
[34] Kojima Y, Usuki A, Kawasumi M, Okada A, Kurauchi T, Kamigaito O, et al. J Polym Sci Part B Polym Phys 1995;33(7):1039–45.
[35] Shelley JS, Mather PT, DeVries KL. Polymer 2001;42(13):5849–58.
[36] Skrovanek DJ, Howe SE, Painter PC, Coleman MM. Macromolecules 1985;18(9):1676–83.
[37] Huang JJ, Keskkula H, Paul DR. Polymer 2004;45(12):4203–15.
[38] Hu YS, Mehta S, Schiraldi DA, Hiltner A, Baer E. J Polym Sci Part B Polym Phys 2005;43(11):1365–81.
[39] Moisa S, Landsberg G, Rittel D, Halary JL. Polymer 2005;46(25):11870–5.
[40] Garcia M, Eguiazabal JI, Nazabal J. Polym Eng Sci 2002;42(2):413–23.
[41] Wunnicke O, Muller-Buschbaum P, Wolkenhauer M, Lorenz-Haas C, Cubitt R, Leiner V, et al. Langmuir 2003;19(20):8511–20.
[42] Granado A, Equizabal JI, Nazabal J. Macromol Mater Eng 2004;289(3):281–7.
[43] Kiersnowski A, Dabrowski P, Budde H, Kressler J, Piglowski J. Eur Polym J 2004;40(11):2591–8.
[44] Chen BQ, Evans JRG. J Phys Chem B 2004;108(39):14986–90.
[45] Agilent Technologies technical brochure 'Process control of polyamide-6,6'.
[46] Mitomo H. J Polym Sci Part B Polym Phys 1988;26(2):467–72.
[47] Morgan AB, Gilman JW. J Appl Polym Sci 2003;87(8):1329–38.
[48] Fornes TD, Yoon PJ, Paul DR. Polymer 2003;44(24):7545–56.
[49] Supplementary material.
[50] Bourbigot S, Gilman JW, Wilkie CA. Polym Degrad Stab 2004;84(3):483–92.
[51] Zong RW, Hu Y, Liu N, Li S, Liao GX. J Appl Polym Sci 2007;104(4):2297–303.
[52] Unpublished data.
[53] Lim ST, Hyun YH, Choi HJ, Jhon MS. Chem Mater 2002;14(4):1839–44.
[54] Xie W, Gao ZM, Pan WP, Hunter D, Singh A, Vaia R. Chem Mater 2001;13(9):2979–90.
[55] Allen NS, Edge M. Fundamentals of polymer degradation and stabilisation. London: Elsevier; 1992.
[56] Villar-Rodil S, Paredes JI, Martinez-Alonso A, Tascon JMD. Chem Mater 2001;13(11):4297–304.
[57] Wu PY, Yang YL, Siesler HW. Polymer 2001;42(26):10181–6.
[58] Do CH, Pearce EM, Bulkin BJ, Reimschuessel HK. J Polym Sci Part A Polym Chem 1986;24(7):1657–74.
[59] Socrates G. Infrared characteristic group frequencies: tables and charts. 3rd ed. Chichester: Wiley; 2001.
[60] Lin-Vien D, Colthup BN, Fateley GW, Grasselli GJ. The handbook of infrared and Raman characteristic frequencies of organic molecules. Boston: Academic Press; 1991.
[61] Shibryaeva LS, Popov AA, Zaikov GE. Thermal oxidation of polymer blends. Leiden: VSP; 2006.
[62] Ballistreri A, Garozzo D, Maravigna P, Montaudo G, Giuffrida M. J Polym Sci Part A Polym Chem 1987;25(4):1049–63.
[63] Do CH, Pearce EM, Bulkin BJ, Reimschuessel HK. J Polym Sci Part A Polym Chem 1987;25(9):2409–24.
[64] Levchik SV, Weil ED, Lewin M. Polym Int 1999;48(7):532–57.
[65] Kalugina EV, Gumargaliveva KZ, Zaikov GE. Thermal stability of engineering heterochain thermoresistant polymers. Netherlands: Brill Academic; 2004.
[66] Farmer VC, Russell JD. Spectrochim Acta 1964;20(7):1149–73.
[67] Madejova J, Komadel P. Clays Clay Miner 2001;49(5):410–32.
[68] Jang BN, Costache M, Wilkie CA. Polymer 2005;46(24):10678–87.
[69] Morgan AB, Wilkie CA. Flame retardant polymer nanocomposites. New Jersey: Wiley; 2007.